ACS APPLIED POLYMER MATERIALS

pubs.acs.org/acsapm Article

Vat Photopolymerization of Supersoft Acrylamide-Based PDMS Bottlebrush Elastomers

Kamyar Karimi Nikoo, James R. Brown, Garvit Nayyar, Timothy E. Long, and Jeffrey L. Self*

Cite This: ACS Appl. Polym. Mater. 2025, 7, 9234−9242 Read Online

ACCESS | Metrics & More | Article Recommendations | Supporting Information

ABSTRACT: Bottlebrush polymers, defined as polymers densely grafted with polymer side chains, have gained much attention for their unique mechanical properties. When cross-linked into a bottlebrush polymer network, these materials exhibit moduli in the kilopascal range, significantly softer than conventional linear polymer networks. The ability to access these "super-soft" materials creates exciting opportunities in fields requiring biointerfacing or highly compliant materials, such as tissue engineering, biomedical devices, and pressure sensors. Additive manufacturing (AM), specifically vat photopolymerization (VPP), provides a platform for the fabrication of a polymer network with precise and bespoke form factors. However, challenges such as high resin viscosity and slow curing rates are known obstacles for integrating bottlebrush polymer chemistry into VPP processes. This study introduces a synthetic approach leveraging acrylamide-terminated poly(dimethylsiloxane) (PDMS) macromonomers and cross-linkers for the VPP manufacturing of supersoft, solvent-free elastomers. These siloxane-based resins exhibit both low viscosity and rapid photocuring, making them ideal materials for VPP. The cross-link density can be directly controlled through formulation design, achieving storage moduli from 10^3 to 10^6 Pa, without necessitating solvent or plasticizer as in conventional systems. The elastomeric response of the photocured materials is evaluated with compression testing, reversibly accessing strains of up to 60%. The quality of the 3D-printed parts is confirmed via scanning electron microscopy. This work offers a practical synthetic route to 3D-printable PDMS-based supersoft elastomers, with modulus values on the order of soft tissue, for next-generation sensors and biointerfacing technologies.

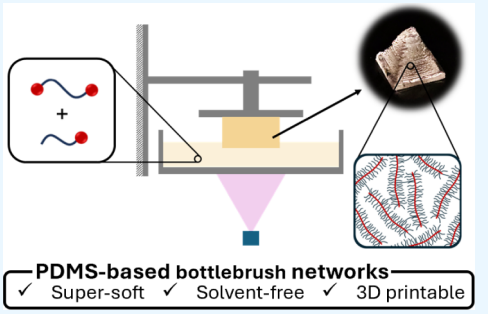

KEYWORDS: *poly(dimethylsiloxane), PDMS, bottlebrush polymer, elastomer, 3D printing, additive manufacturing, vat photopolymerization, acrylamide*

INTRODUCTION

Bottlebrush polymers are macromolecules composed of a main chain ("backbone") whose repeat unit contains a pendant polymer chain ("side chain").[1] As such, these bottlebrush polymers can have molecular weights >1 MDa, creating challenges with their synthesis and characterization. Advances in synthetic methods for the production of polymers with bottlebrush architectures have led to a surge of interest in integrating these novel materials toward engineering applications. One of the most notable attributes of bottlebrush polymers is their ability to form supersoft networks when appropriately cross-linked, with shear moduli in the single kilopascal range at low cross-linking densities. Thus, the stiffness of bottlebrush networks can be orders of magnitude lower than that of conventional linear polymer networks, where network strand entanglements impose a lower limiting modulus (on the order of 1 MPa).[2−6] Previous work has shown that this remarkable property arises as a result of reduced entanglement within the bottlebrush network as well as the high concentration of network defects (dangling side chains).[7] The net result of these effects is a biomimetic material with moduli comparable to soft tissue, as shown in Figure 1. Researchers hoping to leverage this unique property have explored the use of bottlebrush elastomers in applications such as synthetic tissue,[5,8] actuators,[4] pressure sensors,[9] implants,[10] conductive elastomers,[11,12] and 3D printing.[13]

There are three common synthetic routes to obtain bottlebrush polymers: (1) grafting-to, where reactive polymer chains add on to the pre-existing backbone;[18−20] (2) grafting-from, where side chain polymerization initiates from the backbone initiation sites;[21−25] and (3) grafting-through, where polymers with terminal functional groups (i.e., macromonomers) polymerize to yield the final bottlebrush polymer.[6,9,13,26−29] Compared to the first two routes, the grafting-through strategy ensures 100% grafting density by prefunctionalizing all the side chains.[30] As the grafting density heavily influences the properties of complex structural

Received: April 29, 2025
Revised: July 3, 2025
Accepted: July 4, 2025
Published: July 14, 2025

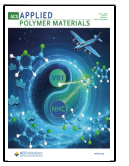

https://doi.org/10.1021/acsapm.5c01527
ACS Appl. Polym. Mater. 2025, 7, 9234−9242

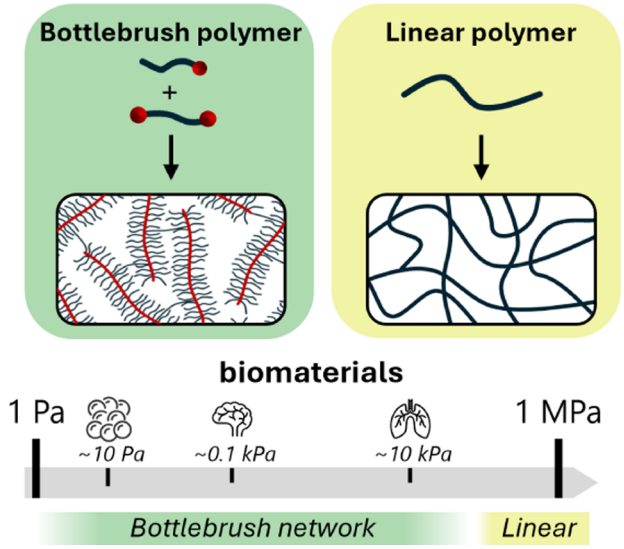

Figure 1. Comparison of accessible modulus values for conventional linear networks and bottlebrush polymer networks, with reference values of relevant biomaterials.[14−17]

polymers, the precise control afforded by the grafting-through method makes it a more suitable choice for investigating structure−property relationship.[31] The most common specific synthetic routes to generate bottlebrush polymers are (1) ruthenium-catalyzed ring-opening metathesis polymerization of norbornene-functionalized macromonomers followed by subsequent cross-linking[9,32−34] and (2) cross-linking of monofunctional and telechelic macromonomers through radical polymerization.[35−37]

Compared to traditional manufacturing methods, additive manufacturing or 3D printing (3DP) enables an accessible, versatile, rapid-prototyping platform with reduced material waste.[38] A variety of 3DP methods have been developed for different classes of materials, including material extrusion-based and vat photopolymerization-based systems for polymeric materials.[39,40] A variant of extrusion-based systems is direct ink writing (DIW), which involves the extrusion of material from a nozzle positioned along three coordinate axes.[41] Bottlebrush polymers, which often have high molecular weights and, thus, high viscosities, are more easily integrated into extrusion-based systems. For example, direct ink writing (DIW) ink viscosity typically falls between 10^2 and 10^6 mPa·s.[42] However, photopolymerization-based methods, such as vat photopolymerization (VPP), have the added benefits of greatly improved resolution, short processing times, and interlayer adhesion with spatial and temporal control over photopolymerization.[43] Conventional VPP resins must be low viscosity for successful printing and are composed of acrylate-, methacrylate-, or acrylamide-based monomer systems coupled with a photoresponsive free-radical initiator.[44] Given the desirable properties that can be achieved with bottlebrush polymers,[45] integration of bottlebrush polymers into a VPP manufacturing mode would enable the production of supersoft elastomers with precise form factors and complex geometries. Existing literature has demonstrated compatible resins for manufacturing bottlebrush materials through both digital light processing (DLP)[36] and UV-assisted DIW.[13]

Here, we report acrylamide-terminated poly(dimethylsiloxane) (PDMS) macromonomers and cross-linkers that enable fast and solvent-free bottlebrush network formation via UV-initiated free-radical polymerization. The synthesis of the major resin components is single-step, scalable (34 g), and high yielding (83%). Compared with other photo-cross-linked bottlebrush polymers,[13,35,36] this chemistry affords sufficiently low viscosity (<1 Pa·s) for easy processing while maintaining rapid curing kinetics. Ultimately, 3D-printed PDMS parts with supersoft and tunable shear moduli (10^6−10^6) and high gel fraction (>85%) are demonstrated.

EXPERIMENTAL SECTION

Materials. Diphenyl(2,4,6-trimethylbenzoyl)phosphine oxide (TPO, 97%) was purchased from TCI. Acryloyl chloride (≥97%), potassium hydroxide, magnesium sulfate (≥98.0%), and chloroform-d ($CDCl_3$, 99.8%) were purchased from Sigma-Aldrich. Monoaminopropyl-terminated poly(dimethylsiloxane) (MCR-A12, 2 kDa) and aminopropyl-terminated poly(dimethylsiloxane) (DMS-A15, 3 kDa) were purchased from Gelest. Chloroform (HPLC grade) and dichloromethane (DCM) (ACS grade) were purchased from Fisher Scientific. All compounds were used as received, except where stated otherwise.

Characterization. Chemical composition data were collected with ^{1}H nuclear magnetic resonance (NMR) spectroscopy performed in $CDCl_3$ on a Bruker Avance NEO at 500 MHz (23 °C) with a 5 mm iProbe, with chemical shifts reported relative to residual solvent signals. All rheology experiments were conducted on a TA Instruments HR-30 rheometer. Photorheological measurements were conducted using a 20 mm parallel plate geometry composed of a disposable aluminum upper plate and a 20 mm quartz lower optical plate, using an Omnicure S2000 high-pressure Hg lamp with 320−500 nm wavelength range as the light source. The irradiation protocol for the photocuring experiments consisted of an initial 30 s dark period followed by a 570 s exposure time (for a total experiment time of 10 min) at an intensity of 11 mW/cm^2—a radiometer was used to confirm the UV light intensity. These measurements were made in oscillatory mode at a 1 Hz frequency and a 1% strain, with "Fast Sampling" enabled to better capture the rapid kinetics. An axial force of approximately 0 N was maintained throughout the experiment. Shear storage plateau moduli (G_N^0) were determined by frequency sweeps in the linear viscoelastic region at a 1% strain. The crossover times (determined to be where $G'/G'' = 1$) were determined by using the "modulus crossover" analysis function in TA Instruments TRIOS software. Viscosity was measured in a flow sweep experiment using 40 mm stainless steel parallel plates. Compression tests (cyclic and noncyclic) were conducted on the rheometer with 20 mm stainless steel parallel plates in the compression mode using a constant deformation rate of 1 μm/s. Toughness values were calculated in Origin by integrating the area under the curve using built-in functions. A Thermo Scientific Phenom XL large-stage scanning electron microscope (SEM) under a backscattering detector, 0.1 Pa vacuum and a 15 kV accelerating voltage, was used for direct visualization of the surface and cross-sections of the 3D printing specimens. Samples were sputter-coated with a 6 nm thin layer of gold and mounted on aluminum stems using carbon tape. The 3D printing was carried out using an Asiga Max X27 DLP printer with no modifications. Parts were printed using a 385 nm UV source at an intensity of 21 mW/cm², a layer thickness of 50 μm, and an exposure time of 5 s.

Synthesis of Mono Acrylamide-Terminated Poly(dimethylsiloxane) (PMDS-AA). The synthesis proceeded according to standard Schotten−Baumann conditions from Sirrine et al. (2018).[46] Proton nuclear magnetic resonance (^{1}H NMR) spectroscopy in $CDCl_3$ enabled determination of PDMS-NH_2 actual M_n (1.7 kDa) after vacuum stripping of low molecular weight cyclic-PDMS impurities. The PDMS-NH_2 (Gelest DMS-A21, 60 g, 30 mmol) was added to a 500 mL, two-necked, round-bottomed flask equipped with a magnetic stir bar, air condenser (Findenser), and addition funnel. After PDMS-NH_2 was dissolved in 200 mL of DCM, 200 mL of aqueous 1 N potassium hydroxide solution was added to the round-

https://doi.org/10.1021/acsapm.5c01527
ACS Appl. Polym. Mater. 2025, 7, 9234−9242

bottomed flask. The reaction vessel was placed in an ice-water bath and purged with nitrogen gas flow for 30 min. To the cooled flask, acryloyl chloride (3.03 mL, 37.5 mmol) was added dropwise under vigorous stirring. After 24 h, the organic phase was charged to a separatory funnel and washed with brine solution (3 × 200 mL). The organic layer was then passed through basic alumina and dried over $MgSO_4$ after which the DCM was removed with a rotary evaporator. The final polymer was dried at 50 °C under a reduced pressure for 18 h. The isolated yield was 55.2 g (92%). The macromonomer chemical structure and percent acrylamide termination were verified with ^{1}H NMR spectroscopy in $CDCl_3$ (Figure S1).

Synthesis of Bis Acrylamide-Terminated Poly(dimethylsiloxane) (PMDS-bisAA). Similar to monoacrylamide-terminated PDMS synthesis, ^{1}H NMR spectroscopy in $CDCl_3$ enabled the determination of PDMS-bisNH_2 actual M_n (3.1 kDa) after vacuum stripping of low molecular weight cyclic-PDMS compounds. PDMS-bisNH_2 (Gelest DMS-A15, 40.6 g, 13.5 mmol) was added to a 500 mL, two-necked, round-bottomed flask equipped with a magnetic stir bar, an air condenser (Findenser), and an addition funnel. After PDMS-bisNH_2 was dissolved in 135 mL of DCM, 135 mL of aqueous 1 N potassium hydroxide solution was added to the round-bottomed flask. The reaction vessel was placed in an ice-water bath and purged with a nitrogen gas flow for 30 min. To the cooled flask, acryloyl chloride (2.72 mL, 33.7 mmol) was added dropwise under vigorous stirring. The workup procedure was identical to the PDMS-NH_2 macromonomer synthesis given above. The final isolated yield was 33.5 g (83%). The cross-linker chemical structure and percent acrylamide termination were verified with ^{1}H NMR spectroscopy in $CDCl_3$ (Figure S2).

Preparation of Photocurable Resins. For each study, resins were prepared in 2-dram scintillation vials comprising PDMS-AA and PDMS-bisAA, totaling 1.00 g, in a specific molar ratio. To these vials, 10 mg of photoinitiator solution (3 wt % TPO in chloroform) was added and homogenized by vortex mixing vigorously for 30 s. The preparation of samples for VPP experiments was identical with that of photorheology samples.

RESULTS AND DISCUSSION

Molecular Design and Synthesis. PDMS exhibits high thermal and thermo-oxidative polymer stability with excellent UV resistance and chemical inertness. Additionally, its high segmental motion and low glass transition temperature (approximately −120 °C) make PDMS a highly desirable elastomer in a wide variety of applications.[47] As such, it is an ideal candidate for this work, aiming to achieve VPP of high-performance elastomers. Similarly, acrylamide-functionalized components would enable photocuring via radical-mediated free radical polymerization (FRP), aided by the rapid kinetics of acrylamide homopolymerization.[48] This approach avoids the use of reactive diluents, heat, and solvent (beyond the minimal solvent necessary to dissolve the photoinitiator, as described in the experimental section). To date, the use of acrylamide chemistry to generate bottlebrush polymer elastomers via photopolymerization remains unexplored.

The single-step synthesis of both the macromonomer and cross-linker from commercially available monofunctionalized amino-PDMS and difunctionalized amino-PDMS, respectively, is shown in Figure 2. Biphasic Schotten−Baumann conditions afford acrylamide-functionalized PDMS from aminopropyl-terminated PDMS and acryloyl chloride. These conditions help increase heat dissipation to prevent premature cross-linking and facilitate the reaction workup by having the generated HCl and acrylic acid to migrate to the aqueous phase for separation. These conditions were also found to be scalable, successfully synthesizing 55.2 g of macromonomer and 33.5 g of cross-linker using a single-step reaction, and highly yielding

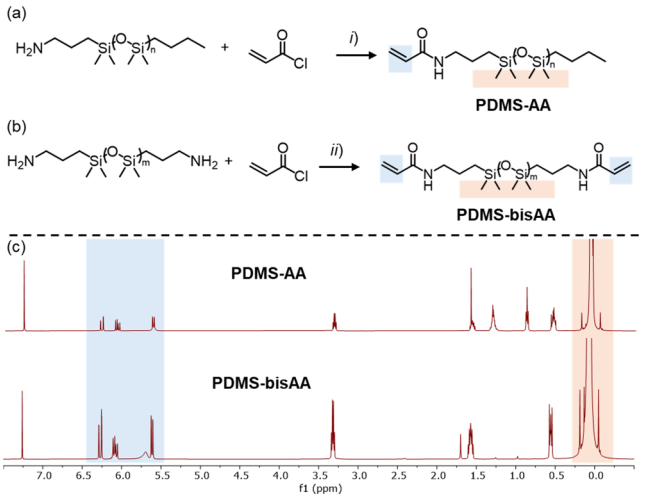

Figure 2. (a) Functionalization of (3-aminopropyl)-terminated PDMS to afford a monofunctional acrylamide-PDMS macromonomer. (b) Functionalization of bis(3-aminopropyl)-terminated PDMS to afford a bifunctional acrylamide-PDMS cross-linker, with conditions given in experimental methods. (c) ^{1}H NMR of PDMS-AA macromonomer and PDMS-bisAA cross-linker. All chemical shifts are referenced to residual solvent peaks.

(affording 92% and 83% yield, respectively). Molecular weights of 2 and 3 kDa were chosen for the macromonomer and cross-linker. Conventional linear polymer melts exhibit molecular weights of entanglement (M_e) starting at 10^3 to 10^4 Da,[49] above which their viscosity (before network formation) and modulus (after network formation) increase drastically. Conversely, polymers with bottlebrush architecture exhibit suppressed entanglement (greatly increased M_e) and reduced viscosity relative to linear polymers of similar molecular weights due to the large volume associated with each network strand and the high concentration of network defects.[50] Strategic choice of molecular weight for the bottlebrush network precursors results in a resin that has sufficiently low viscosity to be compatible with vat photopolymerization while still exhibiting the unique properties of bottlebrush polymer networks after photocuring.

While the NMR data suggest complete functionalization, even small impurities can have dramatic effects on the curing behavior. Primarily, trace amounts of difunctional impurities in a monomer resin can result in gelation instead of the formation of a polymer melt.[51] Photorheology experiments were conducted on both the macromonomer and cross-linker to confirm the absence of gelation for the former and efficient gelation for the latter, as further evidence of their successful synthesis. In this case, TPO (diphenyl(2,4,6-trimethylbenzoyl)phosphine oxide) was chosen as a photoradical initiator to simulate the network curing during VPP. As shown in Figure 3, upon UV irradiation both the macromonomer and cross-linker exhibit rapid increases in their modulus values. In the case of only macromonomer (Figure 3a), there is no crossover, indicating that we are effectively forming bottlebrush polymers that are neither cross-linked nor entangled. This result confirms that the macromonomer is behaving as expected. Complete polymerization of the macromonomer was confirmed using ^{1}H NMR spectroscopy, as highlighted in Figure S3. Conversely, the homopolymerization of the cross-linker is given in Figure 3b, showing a similarly rapid rise in modulus but reaching significantly higher

https://doi.org/10.1021/acsapm.5c01527
ACS Appl. Polym. Mater. 2025, 7, 9234−9242

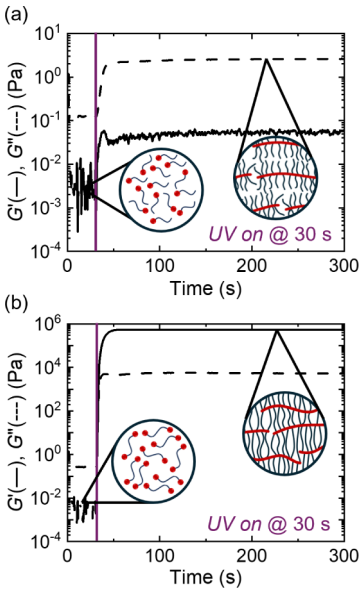

Figure 3. (a) Photorheology for neat PDMS-AA, showing a modest increase in both storage and loss modulus with no crossover point, indicating formation of a bottlebrush polymer melt. (b) Photorheology for neat PDMS-bisAA, showing a significant increase in both moduli with a clear crossover point, indicating formation of a cross-linked polymer network.

values (nearing 10^6 Pa) and undergoing a clear G'/G'' crossover point. This sample represents the highest accessible modulus for this resin system and, notably, approaches a modulus value representative of conventional linear PDMS networks. This crossover point marks the gel point of the polymerization, when the viscoelastic response changes from a viscous-dominated response to an elastic-dominated response, confirming the formation of a percolating network. The significant separation of G' and G'' (over a decade) as well as the formation of a flat plateau in G' at long times indicates that the sample is highly cross-linked.[51] The chemical and rheological characterization of the mono- and bisfunctional PDMS confirm the synthesis of the bottlebrush network resin components.

To explore the property space accessible with this method, a series of samples were made with decreasing amounts of cross-linker relative to the macromonomer. This is a facile way of probing the effect of cross-linker density, which is known to impact the properties of cross-linked networks. This is shown schematically in Figure 4a, wherein the molar ratio of macromonomer to cross-linker is systematically varied from 5:1 (moderately cross-linked) to 40:1 (loosely cross-linked); the network formed solely from cross-linker in Figure 3b then reflects the limit of maximum cross-link density. The curing profiles of these various resins are shown in Figure 4b where it can be seen that the G'/G'' crossover occurs rapidly in all formulations, eventually reaching a plateau G' value that indicates complete conversion. Importantly, modulus values have a known frequency dependence, so the equilibrium plateau modulus (G_N^0) can be measured as the storage modulus value at low-frequency deformation in a frequency sweep.[51] The results of these experiments (Figure 4c) show a monotonic decrease in plateau modulus with decreasing cross-linker loading while maintaining a large separation between G' and G''. This is in agreement with rubber elasticity

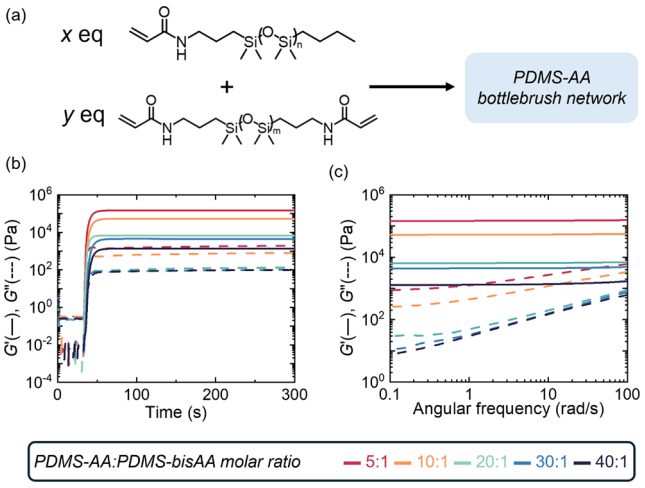

Figure 4. (a) The network components can be formulated with varying relative equivalents to directly control the cross-linking density in the final polymer network. This can be seen in (b) photorheology of a series of formulations shows rapid curing and composition-dependent modulus values and (c) frequency sweeps in the linear viscoelastic region (strain amplitude γ = 0.1%) to approximate the equilibrium plateau modulus (G_N^0).

theory, as the decrease in cross-linking density effectively dilutes the concentration of elastically effective network strands, resulting in a reduction in modulus.[52−54]

From the photorheology and rheology experiments, several key parameters can be extracted for further analysis (Figure 5). The first parameter, plateau modulus (G_N^0), is particularly important as it highlights a distinct feature of bottlebrush polymer networks: modulus values below what is conventionally accessible for linear elastomers (approximately 0.5 MPa for PDMS).[9] With a molar ratio of 40:1 macromonomer to cross-

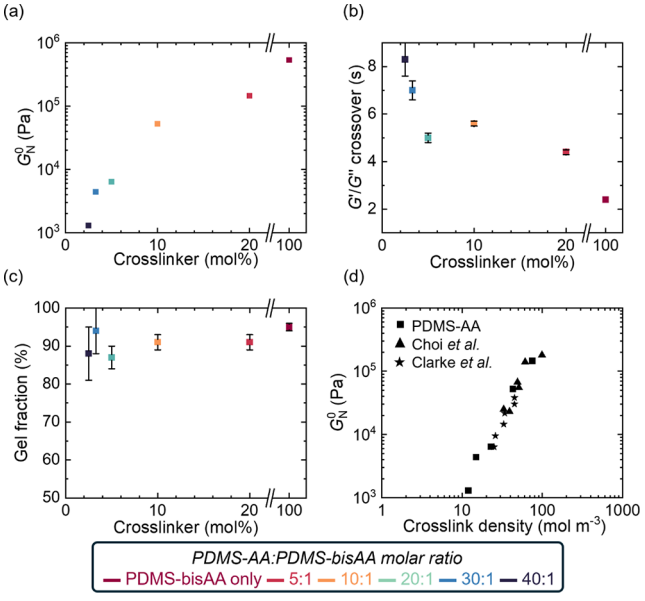

Figure 5. Effect of cross-linker loading on various properties of the photopolymerized bottlebrush resins are shown here, including (a) the trend of increasing plateau modulus, (b) the trend of a decreasing G'/G'' crossover time, (c) a uniform high gel fraction across all loadings, and (d) the plateau modulus of cross-linked bottlebrush networks with PDMS side chains but different backbone chemistries.

https://doi.org/10.1021/acsapm.5c01527
ACS Appl. Polym. Mater. 2025, 7, 9234−9242

linker, modulus values as low as 1.3 kPa can be achieved. Conversely, if only cross-linker is used in the formulation, a modulus value of 0.5 MPa is observed, approximating the typical limit for linear PDMS networks. In the case of conventional radically cured photoresins (typically acrylate-based), the modulus limit is even higher, with values of $G' \geq 1$ MPa.[55,56] To evaluate the suitability for additive manufacturing, the G'/G'' crossover times were measured for each formulation (Figure 5b). These times indicate the minimum irradiation time necessary to transform the liquid resin to a solid or gel-like material. For an efficient 3D printing method, shorter cure times are desirable to minimize processing time. For these resins, rapid crossover times (<10 s) were observed across all tested formulations. The crossover time data reveal a dependence on cross-linker loading, with higher cross-linker loading resulting in faster cure times due to the necessary conversion for network percolation decreasing with increasing prepolymer functionality.[57]

As previously stated, bottlebrush polymers have the advantageous property of reduced modulus as a result of their unique architectural design. However, similarly soft materials can be achieved with linear polymer networks through the inclusion of a plasticizer or solvent in the network. Therefore, to prove that the low modulus is truly a result of the architecture and not of residual solvent or unreacted materials, the gel fractions for photocured samples of each formulation were measured in triplicate. These samples showed a uniform gel fraction of approximately 90%, indicating that the network curing is proceeding to high conversion with only minor residual non-cross-linked bottlebrush. This evidence further supports that the mechanical behavior of our bottlebrush polymer networks is a result of their architecture and not of residual solvent or unreacted plasticizer.

Lastly, we benchmarked our final modulus results against similar radically cured PDMS-based bottlebrush networks presented in the literature. This analysis is given in Figure 5d, where moduli and cross-linking density data from literature reports are plotted for comparison.[35,58] A discussion of cross-link density calculations and the tabulated values is presented in the Supporting Information. All systems exhibit an approximately linear correlation with a similar trend between $\log(G_N^0)$ and log (cross-link density), holding true even at dilute cross-linker loadings. The linearity at low cross-linker loadings supports the claim that contributions from entanglements in these bottlebrush networks are negligible. Furthermore, the magnitude of moduli in these cross-linked networks is in reasonable agreement, reflecting the fact that each network is primarily composed of PDMS, with the slight disagreement between data sets being attributable to differences in bottlebrush backbone chemistry (e.g., acrylate versus acrylamide backbones). Additionally, these results highlight the significant role of side-chain chemistry (as opposed to backbone chemistry) in dictating the modulus of the final network. Overall, Figure 5d provides a quantitative understanding of the connection between formulation and mechanical properties of PDMS bottlebrush systems.

To further probe the properties of these bottlebrush networks, samples were evaluated via compressive strain tests (Figure 6). As evident from the measurements, increasing the cross-linker concentration in the formulation systematically decreases the strain-at-break. This decrease reflects the formation of stiffer and more brittle networks resulting from the higher cross-linker density. Conversely, lowering the cross-

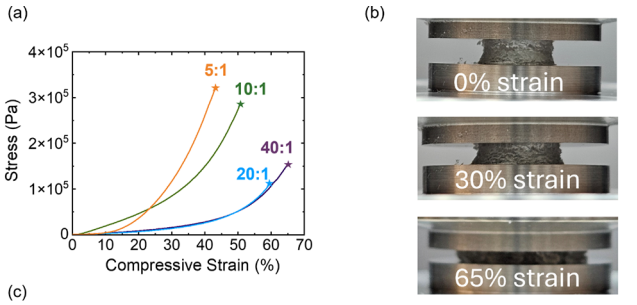

(c)

Sample	Crosslink density (mol m^{-3})	Strain at break (%)	Stress at break (MPa)	Toughness (J.m^{-3}) × 10^{-4}
5:1	75	44 ± 3	0.32 ± 0.07	3.8 ± 0.2
10:1	43	51 ± 1	0.29 ± 0.03	4.4 ± 0.1
20:1	23	60 ± 4	0.11 ± 0.02	1.5 ± 0.1
40:1	12	65 ± 7	0.15 ± 0.03	2.2 ± 0.1

Figure 6. Compressive stress−strain experiments on PDMS-based bottlebrush polymers, including (a) representative traces for each formulation tested, (b) photographs of a sample during compression testing, and (c) tabulated values summarizing the compression experiments.

linker density enables higher ultimate elongations due to improved molecular mobility within the network, while also resulting in lower moduli and higher ductility.[51] A toughness value for each compressive failure is calculated from the area under the stress−strain curve. The extracted parameters of interest, including the calculated cross-link density as discussed in the Supporting Information, strain-at-break, stress-at-break, and toughness, are tabulated in Figure 6c. The softest bottlebrush elastomer tested exhibited a compressive strain-at-break of 65%, approximately the same as a poly(acrylamide) (PAM) hydrogel with a similar modulus.[3] Ultimately, it was observed that while the modulus values are comparable to other bottlebrush networks, the strains at break of these samples are markedly lower than those prepared by more controlled bottlebrush polymerization chemistry, i.e., Grubbs-catalyzed ROMP[15,59] and atom transfer radical polymerization (ATRP).[3,5]

It is known that the mechanical properties of cross-linked networks at high strains are sensitive to network topology.[60] The use of free-radical polymerization (FRP) to form our bottlebrush networks may be the cause of the relative decrease in network elasticity compared to that of conventional ROMP-based networks. The nature of controlled polymerizations makes it possible to achieve a homogeneous cross-linked network that more closely resembles an "ideal" network model, limiting defects and improving toughness.[61,62] On the other hand, FRP-based network curing involves local initiation and rapid propagation/termination, resulting in a network with heterogeneously distributed cross-link densities, increased network defects, and nonuniform segment distributions.[63] We hypothesize that this difference in network formation results in our acrylamide-based bottlebrush networks exhibiting an order-of-magnitude lower toughness in comparison to previously reported PDMS bottlebrush elastomers (~0.2 MJ/m^3) despite having a similar modulus (~2 kPa).[3] Conversely, when comparing to radically cured hydrogels of similar modulus, we find that these bottlebrush polymer networks exhibit higher toughness values.[64,65] It is important to highlight

https://doi.org/10.1021/acsapm.5c01527
ACS Appl. Polym. Mater. 2025, 7, 9234−9242

that these bottlebrush elastomers do not contain any additives or advanced toughening mechanisms to improve their mechanical properties.[66−68] As such, bottlebrush polymer elastomers show great promise in expanding the toolkit of accessible mechanical properties of synthetic polymer systems. The compressive stress−strain data and cyclic compression plots of different photoresin formulations are provided in Figures S4−S7.

Zero-shear viscosity (η_0) values of acrylamide-terminated macromonomer and cross-linker as well as the 20:1 formulation of PDMS-AA and PDMS-bisAA for VPP are given in Table 1. Water and glycerol are presented for reference. It is apparent and intuitive that the 20:1 molar formulation exhibits viscosity between PDMS-AA and PDMS-bisAA (flow sweep data plotted in Figure S8). The viscosity of a VPP resin limits the ultimate throughput of the process, with more viscous resins requiring longer equilibration times between layer exposures. As such, the practical upper limit for VPP resin viscosity is typically reported as 5 Pa·s.[69] It can therefore be seen in Table 1 that both our resin components and our final resin formulation are at least 1 order of magnitude below this viscosity limit. The low viscosity of our resins reflects the fact that the macromonomer (2 kDa) and cross-linker (3 kDa) are both well below the entanglement molecular weight of PDMS (34.5 kDa),[70] thereby limiting chain−chain interactions.

Table 1. Zero-Shear Viscosity (η_0) for Relevant Siloxanes, Reference Materials, and a Representative VPP Resin of PDMS-AA and PDMS-bisAA

Sample	η_0(Pa s)
Water	0.001
PDMS-AA	0.08
20:1 PDMS-AA:PDMS-bisAA	0.11
Glycerol	0.3
PDMS-bisAA	0.40
Sylgard 184 (mixed)	3.5
Sylgard 184 (base)	5.1

Having identified optimal resin formulations with high gel fraction and supersoft modulus, we then demonstrated their efficient 3D photopolymerization by fabricating objects with a commercially available DLP printer (Asiga Max X27 DLP printer). This printer is shown schematically in Figure 7a. The parts were printed by using a 385 nm UV source at an intensity of 21 mW/cm^2, a layer thickness of 50 μm, and an exposure time of 5 s for the best in-plane resolution. To demonstrate the printing capability, a 2D template was printed as well as a 3D pyramid (Figure 7b). SEM images of the surface and cross-section of the 3D-printed parts are depicted in Figure 7c. The printed parts have a relatively flat surface morphology with no significant defects nor cracks. The DLP printing was conducted in a layer-by-layer manner, and Moiré patterns are visible in SEM images taken by further magnification. Cross-sectional morphology of the printed parts confirmed the cured layer thickness of ∼50 μm as predetermined, while the small deviations may be attributed to UV light scattering during the resin curing process. These results demonstrated the ability to generate geometrically complex structures with good resolution in a vat photopolymerization manufacturing mode utilizing a bespoke bottlebrush network resin.

CONCLUSION

This study demonstrates the successful synthesis, characterization, and additive manufacturing of supersoft, solvent-free, siloxane-based bottlebrush elastomers. By leveraging a low-viscosity resin formulation optimized for VPP, we introduce a new method for the 3D printing of bottlebrush polymer networks. Investigating macromonomer-to-cross-linker molar ratios in the formulation enabled precise control over network properties, resulting in a wide range of tunable shear moduli spanning from 10^6 to 10^3 Pa. This tunability arises from the interplay between chain extension and cross-linking, driven by the free radical polymerization of acrylamide groups. Photorheological studies confirmed rapid curing kinetics with gel

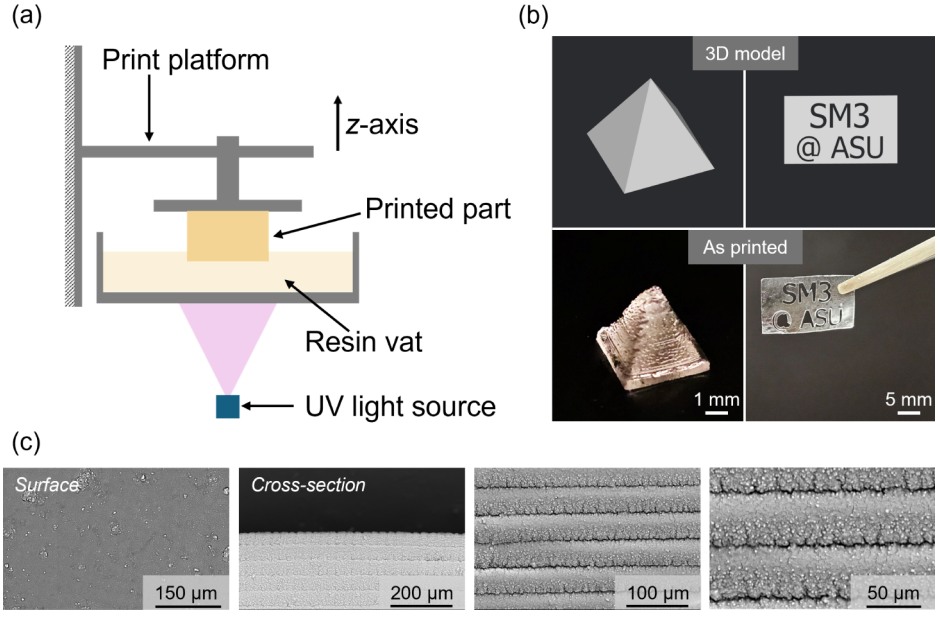

Figure 7. (a) Schematic of a commercially available VPP printer. (b) Images of the 3D printed PDMS-AA bottlebrush parts and their corresponding 3D models. (c) SEM images of the surface and cross-sectional views of a 3D-printed part at varying magnification.

https://doi.org/10.1021/acsapm.5c01527
ACS Appl. Polym. Mater. 2025, 7, 9234−9242

fractions exceeding 85% across all formulations. Compression testing revealed that the bottlebrush elastomers exhibit remarkable softness and sufficient toughness, outperforming traditional hydrogels of comparable moduli. This enhanced mechanical behavior is attributed to the unique architecture of bottlebrush polymers, which minimizes entanglement and allows for higher molecular mobility. The compression tests further highlighted the ability to fine-tune the material's elasticity and toughness.

Lastly, the successful fabrication of complex geometries using a commercially available DLP printer underscores the practicality of this approach. As confirmed by SEM imaging, printed parts displayed excellent layer adhesion and maintained their structure, demonstrating the feasibility of producing high-resolution, supersoft elastomeric objects. Additionally, the solvent-free nature of the resin formulation reduces the environmental impact and simplifies processing, aligning with sustainable manufacturing principles.

Overall, this work contributes to a broader understanding of structure−property relationships in bottlebrush polymers and highlights their potential as a versatile material platform for emerging applications. The ability to fabricate supersoft, solvent-free elastomers with tunable mechanical properties and complex designs opens new avenues for developing biomimetic materials, flexible electronics, and soft robotics. Future work can build on these findings by exploring additional polymerization chemistries and processing techniques to further enhance the performance and applicability of bottlebrush elastomers. Investigating these materials' long-term aging, biocompatibility, and environmental resistance is crucial for expanding their utility. The innovations presented in this study pave the way for the development of next-generation soft materials with practical applications through AM.

■ ASSOCIATED CONTENT

Supporting Information

The Supporting Information is available free of charge at https://pubs.acs.org/doi/10.1021/acsapm.5c01527.

^{1}H NMR spectra of PDMS-AA and PDMS-bisAA, compression data and cyclic compression loading/unloading performance of photocured samples, viscosity of PDMS-AA formulations, cross-link density calculations, and Young's modulus (E) and shear modulus (G) calculations (PDF)

■ AUTHOR INFORMATION

Corresponding Author

Jeffrey L. Self − *School for the Engineering of Matter, Transport, and Energy, Arizona State University, Tempe, Arizona 85287, United States; Biodesign Center for Sustainable Macromolecular Materials and Manufacturing (SM3), Arizona State University, Tempe, Arizona 85287, United States*; Email: jeffreyself@asu.edu

Authors

Kamyar Karimi Nikoo − *School for the Engineering of Matter, Transport, and Energy, Arizona State University, Tempe, Arizona 85287, United States; Biodesign Center for Sustainable Macromolecular Materials and Manufacturing (SM3), Arizona State University, Tempe, Arizona 85287, United States;* orcid.org/0009-0005-1499-1102

James R. Brown − *School of Molecular Sciences and Biodesign Center for Sustainable Macromolecular Materials and Manufacturing (SM3), Arizona State University, Tempe, Arizona 85287, United States*

Garvit Nayyar − *School for the Engineering of Matter, Transport, and Energy, Arizona State University, Tempe, Arizona 85287, United States; Biodesign Center for Sustainable Macromolecular Materials and Manufacturing (SM3), Arizona State University, Tempe, Arizona 85287, United States;* orcid.org/0000-0003-0535-8952

Timothy E. Long − *School for the Engineering of Matter, Transport, and Energy, Arizona State University, Tempe, Arizona 85287, United States; School of Molecular Sciences and Biodesign Center for Sustainable Macromolecular Materials and Manufacturing (SM3), Arizona State University, Tempe, Arizona 85287, United States;* orcid.org/0000-0001-9515-5491

Complete contact information is available at: https://pubs.acs.org/10.1021/acsapm.5c01527

Author Contributions

K.N. and J.B. performed the chemical synthesis. K.N. and G.N. performed the 3D printing. K.N. performed the characterization experiments and analyzed the data. K.N. and J.S. designed the experiments and wrote the manuscript. All authors contributed to reviewing and editing of the manuscript and approved the final version.

Funding

This work was primarily supported by funds from ASU's School for Engineering of Matter, Transport, and Energy. Funding support was also provided by the Biodesign Center for Sustainable Macromolecular Materials and Manufacturing.

Notes

The authors declare no competing financial interest.

■ ACKNOWLEDGMENTS

This work was performed at the Biodesign Center for Sustainable Macromolecular Materials and Manufacturing and its shared facility. The authors would like to thank Renxuan Xie, Ren H. Bean, Benjamin Agbo, Sophia Pedersen, and Addison Sanora for contributing to this work. The authors also thank Brian R. Cherry and Samrat Amin at ASU's Magnetic Resonance Research Center.

■ REFERENCES

(1) Dutta, S.; Wade, M. A.; Walsh, D. J.; Guironnet, D.; Rogers, S. A.; Sing, C. E. Dilute solution structure of bottlebrush polymers. *Soft Matter* **2019**, *15* (14), 2928−2941.

(2) Cai, L.-H.; Kodger, T. E.; Guerra, R. E.; Pegoraro, A. F.; Rubinstein, M.; Weitz, D. A. Soft Poly(dimethylsiloxane) Elastomers from Architecture-Driven Entanglement Free Design. *Adv. Mater.* **2015**, *27* (35), 5132−5140.

(3) Daniel, W. F. M.; Burdyńska, J.; Vatankhah-Varnoosfaderani, M.; Matyjaszewski, K.; Paturej, J.; Rubinstein, M.; Dobrynin, A. V.; Sheiko, S. S. Solvent-free, supersoft and superelastic bottlebrush melts and networks. *Nat. Mater.* **2016**, *15* (2), 183−189.

(4) Vatankhah-Varnoosfaderani, M.; Daniel, W. F. M.; Zhushma, A. P.; Li, Q.; Morgan, B. J.; Matyjaszewski, K.; Armstrong, D. P.; Spontak, R. J.; Dobrynin, A. V.; Sheiko, S. S. Bottlebrush Elastomers: A New Platform for Freestanding Electroactuation. *Adv. Mater.* **2017**, *29* (2), 1604209.

(5) Vatankhah-Varnosfaderani, M.; Daniel, W. F. M.; Everhart, M. H.; Pandya, A. A.; Liang, H.; Matyjaszewski, K.; Dobrynin, A. V.;

Sheiko, S. S. Mimicking biological stress−strain behaviour with synthetic elastomers. *Nature* **2017**, *549* (7673), 497−501.
(6) Mukherjee, S.; Xie, R.; Reynolds, V. G.; Uchiyama, T.; Levi, A. E.; Valois, E.; Wang, H.; Chabinyc, M. L.; Bates, C. M. Universal Approach to Photo-Crosslink Bottlebrush Polymers. *Macromolecules* **2020**, *53* (3), 1090−1097.
(7) Hu, M.; Xia, Y.; McKenna, G. B.; Kornfield, J. A.; Grubbs, R. H. Linear Rheological Response of a Series of Densely Branched Brush Polymers. *Macromolecules* **2011**, *44* (17), 6935−6943.
(8) Vatankhah-Varnosfaderani, M.; Keith, A. N.; Cong, Y.; Liang, H.; Rosenthal, M.; Sztucki, M.; Clair, C.; Magonov, S.; Ivanov, D. A.; Dobrynin, A. V.; Sheiko, S. S. Chameleon-like elastomers with molecularly encoded strain-adaptive stiffening and coloration. *Science* **2018**, *359* (6383), 1509−1513.
(9) Reynolds, V. G.; Mukherjee, S.; Xie, R.; Levi, A. E.; Atassi, A.; Uchiyama, T.; Wang, H.; Chabinyc, M. L.; Bates, C. M. Super-soft solvent-free bottlebrush elastomers for touch sensing. *Mater. Horiz.* **2020**, *7* (1), 181−187.
(10) Hu, X.; Zhou, J.; Vatankhah-Varnosfaderani, M.; Daniel, W. F. M.; Li, Q.; Zhushma, A. P.; Dobrynin, A. V.; Sheiko, S. S. Programming temporal shapeshifting. *Nat. Commun.* **2016**, *7* (1), 12919.
(11) Self, J. L.; Reynolds, V. G.; Blankenship, J.; Mee, E.; Guo, J.; Albanese, K.; Xie, R.; Hawker, C. J.; de Alaniz, J. R.; Chabinyc, M. L.; Bates, C. M. Carbon Nanotube Composites with Bottlebrush Elastomers for Compliant Electrodes. *ACS Polym. Au* **2022**, *2* (1), 27−34.
(12) Xu, P.; Wang, S.; Lin, A.; Min, H. K.; Zhou, Z.; Dou, W.; Sun, Y.; Huang, X.; Tran, H.; Liu, X. Conductive and elastic bottlebrush elastomers for ultrasoft electronics. *Nat. Commun.* **2023**, *14* (1), 623.
(13) Xie, R.; Mukherjee, S.; Levi, A. E.; Reynolds, V. G.; Wang, H.; Chabinyc, M. L.; Bates, C. M. Room temperature 3D printing of Super-soft and solvent-free elastomers. *Sci. Adv.* **2020**, *6* (46), No. eabc6900.
(14) Sheiko, S. S.; Dobrynin, A. V. Architectural Code for Rubber Elasticity: From Supersoft to Superfirm Materials. *Macromolecules* **2019**, *52* (20), 7531−7546.
(15) Cater, H. L.; Allen, M. J.; Linnell, M. I.; Rylski, A. K.; Wu, Y.; Lien, H.-M.; Mangolini, F.; Freeman, B. D.; Page, Z. A. Supersoft Norbornene-Based Thermoplastic Elastomers with High Strength and Upper Service Temperature. *Adv. Mater.* **2024**, *36* (30), 2402431.
(16) Cho, K. W.; Sunwoo, S.-H.; Hong, Y. J.; Koo, J. H.; Kim, J. H.; Baik, S.; Hyeon, T.; Kim, D.-H. Soft Bioelectronics Based on Nanomaterials. *Chem. Rev.* **2022**, *122* (5), 5068−5143.
(17) Anseth, K. S.; Bowman, C. N.; Brannon-Peppas, L. Mechanical properties of hydrogels and their experimental determination. *Biomaterials* **1996**, *17* (17), 1647−1657.
(18) Lu, X.; Watts, E.; Jia, F.; Tan, X.; Zhang, K. Polycondensation of Polymer Brushes via DNA Hybridization. *J. Am. Chem. Soc.* **2014**, *136* (29), 10214−10217.
(19) Gao, H.; Matyjaszewski, K. Synthesis of Molecular Brushes by "Grafting onto" Method: Combination of ATRP and Click Reactions. *J. Am. Chem. Soc.* **2007**, *129* (20), 6633−6639.
(20) Yang, L.-C.; Han, L.; Ma, H.-W.; Liu, P.-B.; Shen, H.-Y.; Li, C.; Zhang, S.-B.; Li, Y. Synthesis of Alkyne-functionalized Polymers via Living Anionic Polymerization and Investigation of Features during the Post-"thiol-yne" Click Reaction. *Chin. J. Polym. Sci.* **2019**, *37* (9), 841−850.
(21) Liu, Y.; Chen, P.; Li, Z. Molecular Bottlebrushes with Polypeptide Backbone Prepared via Ring-Opening Polymerization of NCA and ATRP. *Macromol. Rapid Commun.* **2012**, *33* (4), 287−295.
(22) Chen, Y.; Zhou, H.; Sun, Z.; Li, H.; Huang, H.; Liu, L.; Chen, Y. Shell of amphiphilic molecular bottlebrush matters as unimolecular micelle. *Polymer* **2018**, *149*, 316−324.
(23) Zheng, Z.; Ling, J.; Müller, A. H. E. Revival of the R-Group Approach: A "CTA-shuttled" Grafting from Approach for Well-Defined Cylindrical Polymer Brushes via RAFT Polymerization. *Macromol. Rapid Commun.* **2014**, *35* (2), 234−241.
(24) Cheng, C.; Khoshdel, E.; Wooley, K. L. One-Pot Tandem Synthesis of a Core−Shell Brush Copolymer from Small Molecule Reactants by Ring-Opening Metathesis and Reversible Addition−Fragmentation Chain Transfer (Co)polymerizations. *Macromolecules* **2007**, *40* (7), 2289−2292.
(25) Rzayev, J. Synthesis of Polystyrene−Polylactide Bottlebrush Block Copolymers and Their Melt Self-Assembly into Large Domain Nanostructures. *Macromolecules* **2009**, *42* (6), 2135−2141.
(26) Self, J. L.; Sample, C. S.; Levi, A. E.; Li, K.; Xie, R.; De Alaniz, J. R.; Bates, C. M. Dynamic Bottlebrush Polymer Networks: Self-Healing in Super-Soft Materials. *J. Am. Chem. Soc.* **2020**, *142* (16), 7567−7573.
(27) Xie, G.; Martinez, M. R.; Olszewski, M.; Sheiko, S. S.; Matyjaszewski, K. Molecular Bottlebrushes as Novel Materials. *Biomacromolecules* **2019**, *20* (1), 27−54.
(28) Abbasi, M.; Faust, L.; Wilhelm, M. Comb and Bottlebrush Polymers with Superior Rheological and Mechanical Properties. *Adv. Mater.* **2019**, *31* (26), 1806484.
(29) Sheiko, S. S.; Sumerlin, B. S.; Matyjaszewski, K. Cylindrical molecular brushes: Synthesis, characterization, and properties. *Prog. Polym. Sci.* **2008**, *33* (7), 759−785.
(30) Tonge, C. M.; Sauvé, E. R.; Cheng, S.; Howard, T. A.; Hudson, Z. M. Multiblock Bottlebrush Nanofibers from Organic Electronic Materials. *J. Am. Chem. Soc.* **2018**, *140* (37), 11599−11603.
(31) Levi, A. E.; Lequieu, J.; Horne, J. D.; Bates, M. W.; Ren, J. M.; Delaney, K. T.; Fredrickson, G. H.; Bates, C. M. Miktoarm Stars via Grafting-Through Copolymerization: Self-Assembly and the Star-to-Bottlebrush Transition. *Macromolecules* **2019**, *52* (4), 1794−1802.
(32) Cater, H. L.; Balynska, I.; Allen, M. J.; Freeman, B. D.; Page, Z. A. User Guide to Ring-Opening Metathesis Polymerization of endo-Norbornene Monomers with Chelated Initiators. *Macromolecules* **2022**, *55* (15), 6671−6679.
(33) Cater, H. L.; Allen, M. J.; Linnell, M. I.; Rylski, A. K.; Wu, Y.; Lien, H. M.; Mangolini, F.; Freeman, B. D.; Page, Z. A. Supersoft Norbornene-Based Thermoplastic Elastomers with High Strength and Upper Service Temperature. *Adv. Mater.* **2024**, *36* (30), No. e2402431.
(34) Radzinski, S. C.; Foster, J. C.; Matson, J. B. Preparation of Bottlebrush Polymers via a One-Pot Ring-Opening Polymerization (ROP) and Ring-Opening Metathesis Polymerization (ROMP) Grafting-Through Strategy. *Macromol. Rapid Commun.* **2016**, *37* (7), 616−621.
(35) Choi, C.; Self, J. L.; Okayama, Y.; Levi, A. E.; Gerst, M.; Speros, J. C.; Hawker, C. J.; Read de Alaniz, J.; Bates, C. M. Light-Mediated Synthesis and Reprocessing of Dynamic Bottlebrush Elastomers under Ambient Conditions. *J. Am. Chem. Soc.* **2021**, *143* (26), 9866−9871.
(36) Choi, C.; Okayama, Y.; Morris, P. T.; Robinson, L. L.; Gerst, M.; Speros, J. C.; Hawker, C. J.; Read de Alaniz, J.; Bates, C. M. Digital Light Processing of Dynamic Bottlebrush Materials. *Adv. Funct. Mater.* **2022**, *32* (25), 2200883.
(37) Lee, D.; Wang, H.; Jiang, S.-Y.; Verduzco, R. Versatile Light-Mediated Synthesis of Degradable Bottlebrush Polymers Using α-Lipoic Acid. *Angew. Chem., Int. Ed.* **2024**, *63* (48), No. e202409323.
(38) Herzberger, J.; Sirrine, J. M.; Williams, C. B.; Long, T. E. Polymer Design for 3D Printing Elastomers: Recent Advances in Structure, Properties, and Printing. *Prog. Polym. Sci.* **2019**, *97*, 101144.
(39) Bagheri, A.; Jin, J. Photopolymerization in 3D Printing. *ACS Appl. Polym. Mater.* **2019**, *1* (4), 593−611.
(40) Lewis, J. A.; Gratson, G. M. Direct writing in three dimensions. *Mater. Today* **2004**, *7* (7), 32−39.
(41) Lewis, J. A. Direct Ink Writing of 3D Functional Materials. *Adv. Funct. Mater.* **2006**, *16* (17), 2193−2204.
(42) Saadi, M.; Maguire, A.; Pottackal, N. T.; Thakur, M. S. H.; Ikram, M. M.; Hart, A. J.; Ajayan, P. M.; Rahman, M. M. Direct ink writing: a 3D printing technology for diverse materials. *Adv. Mater.* **2022**, *34* (28), 2108855.
(43) Subedi, S.; Liu, S.; Wang, W.; Naser Shovon, S. M. A.; Chen, X.; Ware, H. O. T. Multi-material vat photopolymerization 3D

https://doi.org/10.1021/acsapm.5c01527
ACS Appl. Polym. Mater. 2025, 7, 9234−9242

printing: a review of mechanisms and applications. n*pj. Adv. Manuf.* **2024**, *1* (1), 9.
(44) Zhang, F.; Zhu, L.; Li, Z.; Wang, S.; Shi, J.; Tang, W.; Li, N.; Yang, J. The recent development of vat photopolymerization: A review. *Addit. Manuf.* **2021**, *48*, 102423.
(45) Li, Z.; Tang, M.; Liang, S.; Zhang, M.; Biesold, G. M.; He, Y.; Hao, S.-M.; Choi, W.; Liu, Y.; Peng, J.; Lin, Z. Bottlebrush polymers: From controlled synthesis, self-assembly, properties to applications. *Prog. Polym. Sci.* **2021**, *116*, 101387.
(46) Sirrine, J. M.; Meenakshisundaram, V.; Moon, N. G.; Scott, P. J.; Mondschein, R. J.; Weiseman, T. F.; Williams, C. B.; Long, T. E. Functional siloxanes with photo-activated, simultaneous chain extension and crosslinking for lithography-based 3D printing. *Polymer* **2018**, *152*, 25−34.
(47) Nikoo, K. K.; Dvornic, P. R.; Self, J. L.; Long, T. E. Siloxane-containing polymers: from synthesis and characterization to advanced applications and sustainability, *Polym. Int.*, 2025. DOI: .
(48) Buback, M.; Schroeder, H.; Kattner, H. Detailed kinetic and mechanistic insight into radical polymerization by spectroscopic techniques. *Macromolecules* **2016**, *49* (9), 3193−3213.
(49) Patel, S. K.; Malone, S.; Cohen, C.; Gillmor, J. R.; Colby, R. H. Elastic modulus and equilibrium swelling of poly(dimethylsiloxane) networks. *Macromolecules* **1992**, *25* (20), 5241−5251.
(50) Rubinstein, M.; Colby, R. H. *Polymer physics*; Oxford University Press, 2003.
(51) Hiemenz, P. C.; Lodge, T. *Polymer chemistry*; CRC Press, 2007.
(52) Kato, K.; Ikeda, Y.; Ito, K. Direct Determination of Cross-Link Density and Its Correlation with the Elastic Modulus of a Gel with Slidable Cross-Links. *ACS Macro Lett.* **2019**, *8* (6), 700−704.
(53) Wang, Z.; Volinsky, A. A.; Gallant, N. D. Crosslinking effect on polydimethylsiloxane elastic modulus measured by custom-built compression instrument. *J. Appl. Polym. Sci.* **2014**, *131* (22), 41050.
(54) Flory, P. J.; Rehner, J. Statistical Mechanics of Cross-Linked Polymer Networks II. Swelling. *J. Chem. Phys.* **1943**, *11* (11), 521−526.
(55) Borrello, J.; Nasser, P.; Iatridis, J.; Costa, K. D. 3D Printing a Mechanically-Tunable Acrylate Resin on a Commercial DLP-SLA Printer. *Addit. Manuf.* **2018**, *23*, 374−380.
(56) Lebedevaite, M.; Talacka, V.; Ostrauskaite, J. High biorenewable content acrylate photocurable resins for DLP 3D printing. *J. Appl. Polym. Sci.* **2021**, *138* (16), 50233.
(57) Winter, H. H. Can the gel point of a cross-linking polymer be detected by the G′−G ″crossover? *Polym. Eng. Sci.* **1987**, *27* (22), 1698−1702.
(58) Clarke, B. R.; Kim, H.; Ilton, M.; Watkins, J. J.; Crosby, A. J.; Tew, G. N. The Impact of Polymerization Chemistry on the Mechanical Properties of Poly(dimethylsiloxane) Bottlebrush Elastomers. *Macromolecules* **2022**, *55* (23), 10312−10319.
(59) Cushman, K.; Keith, A.; Tanaka, J.; Sheiko, S. S.; You, W. Investigating the Stress−Strain Behavior in Ring-Opening Metathesis Polymerization-Based Brush Elastomers. *Macromolecules* **2021**, *54* (18), 8365−8371.
(60) Zhang, Z.; Krajniak, J.; Dookhith, A. Z.; Tian, Y.; Sachar, H. S.; Marioni, N.; Duncan, T. J.; Liu, J.; Sanoja, G. E.; Ganesan, V. Topology and Mechanical Properties of Polymer Networks Formed under Free Radical and Atom Transfer Radical Polymerizations. *Macromolecules* **2025**, *58* (6), 3168−3187.
(61) Matyjaszewski, K. Atom Transfer Radical Polymerization (ATRP): Current Status and Future Perspectives. *Macromolecules* **2012**, *45* (10), 4015−4039.
(62) Cho, Y. E.; Lee, S.; Ma, S. J.; Sun, J.-Y. Network design for soft materials: Addressing Elasticity and Fracture Resistance Challenges. *Soft Matter* **2025**, *21* (9), 1603−1623.
(63) Yu, Q.; Xu, S.; Zhang, H.; Ding, Y.; Zhu, S. Comparison of reaction kinetics and gelation behaviors in atom transfer, reversible addition−fragmentation chain transfer and conventional free radical copolymerization of oligo(ethylene glycol) methyl ether methacrylate and oligo(ethylene glycol) dimethacrylate. *Polymer* **2009**, *50* (15), 3488−3494.
(64) Gong, J. P.; Katsuyama, Y.; Kurokawa, T.; Osada, Y. Double-Network Hydrogels with Extremely High Mechanical Strength. *Adv. Mater.* **2003**, *15* (14), 1155−1158.
(65) Peppas, N. A.; Huang, Y.; Torres-Lugo, M.; Ward, J. H.; Zhang, J. Physicochemical foundations and structural design of hydrogels in medicine and biology. *Annu. Rev. Biomed. Eng.* **2000**, *2*, 9−29.
(66) Hausladen, M. M.; Gorbea, G. D.; Francis, L. F.; Ellison, C. J. UV-Assisted Direct Ink Writing of Dual-Cure Polyurethanes. *ACS Appl. Polym. Mater.* **2024**, *6* (4), 2253−2265.
(67) Yirmibesoglu, O. D.; Simonsen, L. E.; Manson, R.; Davidson, J.; Healy, K.; Menguc, Y.; Wallin, T. Multi-material direct ink writing of photocurable elastomeric foams. *Commun. Mater.* **2021**, *2* (1), 82.
(68) Wallin, T. J.; Simonsen, L.-E.; Pan, W.; Wang, K.; Giannelis, E.; Shepherd, R. F.; Mengüç, Y. 3D printable tough silicone double networks. *Nat. Commun.* **2020**, *11* (1), 4000.
(69) Melchels, F. P. W.; Feijen, J.; Grijpma, D. W. A review on stereolithography and its applications in biomedical engineering. *Biomaterials* **2010**, *31* (24), 6121−6130.
(70) Dvornic, P. R.; Jovanovic, J. D.; Govedarica, M. N. On the critical molecular chain length of polydimethylsiloxane. *J. Appl. Polym. Sci.* **1993**, *49* (9), 1497−1507.

https://doi.org/10.1021/acsapm.5c01527
ACS Appl. Polym. Mater. 2025, 7, 9234−9242